Helmholtz-Zentrum Dresden-Rossendorf (HZDR)

Effect of deposition current density on the Co–Ni/SiO2 alloy composite coatings Using Scanning Jet Electrodeposition

Jiang, W.; Qiu, M.; Shen, L.; Lou, G.; Yang, X.; Eckert, K.; Tian, Z.;

Effect of deposition current density on the Co–Ni/SiO₂ alloy composite coatings Using Scanning Jet Electrodeposition

Wei Jiang[1,2,3,§], Mingbo Qiu[1,§], Lida Shen[1], Guibin Lou[1], Xuegeng Yang[2,3], Kerstin Eckert[2,3], Zongjun Tian[1,*].

[1] *National Key Laboratory of Science and Technology on Helicopter Transmission, Nanjing University of Aeronautics and Astronautics, 210016, Nanjing, P. R. China*

[2] *Institute of Fluid Dynamics, Helmholtz-Zentrum Dresden-Rossendorf (HZDR), 01328, Dresden, Germany*

[3] *Institute of Process Engineering，Technische Universität Dresden, 01069, Dresden, Germany*

§ Both authors contributed equally to this work.

* Corresponding author: Zongjun Tian, tianzj@nuaa.edu.cn.

Abstract: Co–Ni/SiO₂ alloy composite coatings were electrodeposited on copper substrate by scanning jet electrodeposition at various current densities to study its effect on the morphologies, texture orientation, microhardness, adhesion force, wear resistance, and corrosion resistance of Co–Ni/SiO₂ alloy composite coatings. The structure and performance of the material were characterized using a scanning electron microscope, XRD diffractometer, nanoindentation, scratch tester, friction and wear tester, and electrochemical methods. The morphologies of the Co–Ni/SiO₂ alloy composite coatings changed from sparse and slender structures to dense starfish structures with an increase in current density. A part of Co precipitated in the form of a face-centered cubic structure and formed a solid solution with Ni, while another part of Co precipitated in the structure of the composite coating in the form of a hexagonal close-packed structure. The Co–Ni/SiO₂ alloy composite coating exhibited excellent adhesion force, wear resistance, and corrosion resistance when the deposition current density was 130 A/dm². Once the current density was exceeded, some microcracks appeared on the surface of the composite coating, after which the adhesion force and corrosion resistance decreased. The present study suggests that current density at 130 A/dm² is more suitable than low current density for jet electrodeposition to prepare high-density and high-quality composite coating.

Keywords: Co–Ni/SiO₂; Scanning jet electrodeposition; Deposition current density.

1 Introduction

Cobalt–Nickel (Co–Ni) alloy composite coatings have been widely used in the surface protection of engineering materials in recent years, due to their excellent mechanical, physical, and chemical properties [1–5]. Electrodeposition is a simple and economical manufacturing process and successfully in preparing numerous metal alloy composite coatings [6–10]. Jet electrodeposition is a circulating solution flow type of electrodeposition. Since it enables a selective localized deposition that can be used for the mobile repair of mechanical parts, jet electrodeposition has recently been widely considered by researchers [11–19]. The latter can improve the current density but can encourage tip discharge, thereby reducing the uniformity and flatness of the coatings. Researchers have used auxiliary processes to improve the growth uniformity of coatings [16–18]. C. Wang [15] proposed rotary interlaced jet electrodeposition to prepare Ni–CeO₂ nanocomposite coatings, using the rotating process to refresh the electrode surface discharge and to achieve uniform growth of the composite coatings. Y. Wang [16] used friction assisted jet electrodeposition to remove sharp points in the growth of the Ni–SiO₂ nanocomposite coatings. W. Jiang [17] improved the uniformity of discharge on the surface of the jet electrodeposition by a magnetic field. K. Zhao [18] prepared a Ni–Al₂O₃ composite coating with good uniformity through an intermittent discharge in jet electrodeposition. Q.

Zhang [19] studied the effect of different flow rates and changes in the content of Co^{2+} and Ni^{2+} in the electrolyte on the deposition of Ni–Co alloy composite coatings.

In this work, the impact of higher current densities on jet electrodeposition has been explored for the first time. The resulting alloy composite coatings have been analyzed in terms of morphologies, microhardness, adhesion force, wear resistance, and corrosion resistance.

2 Experimental

2.1 Experimental setup

Fig. 1a shows the scanning motion diagram of the jet electrodeposition experimental system, Fig. 1b is a photo of the actual processing equipment. The device includes a control system, heating equipment, transmission system, power supply, and nozzle structure. Before the deposition processing experiment, the sample was fixed on the cathode stage, and the machining gap was adjusted by the computer control system. At the same time, the control system moved along the horizontal direction. Then, the electrolyte was pumped out from the storage tank and sprayed on the cathode surface through the pipe. The electrolyte was recycled repeatedly, and a filter screen was installed near the nozzle outlet to prevent the anode slag from blocking the flow channel. Finally, the external power supply was connected, and the nozzle realized synchronous scanning jet electrodeposition.
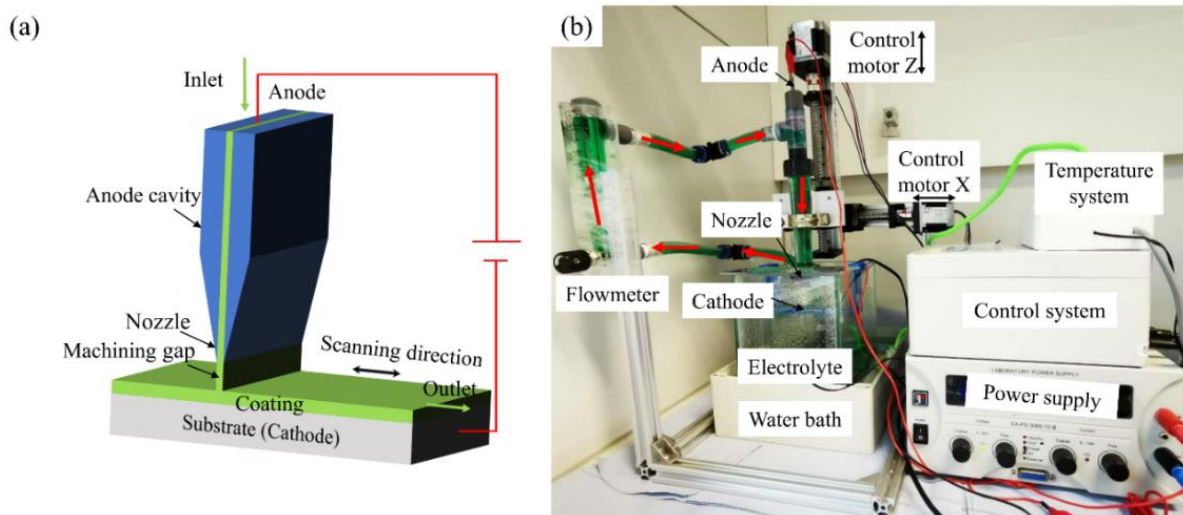

Fig. 1. Scanning Jet Electrodeposition System: (a) schematic diagram, (b) photograph of the setup.

2.2 Parameters

The electrolyte composed of 1.0 M $NiSO_4$, 0.2 M $NiCl_2$, 0.2M $CoSO_4$ and 0.6 M H_3BO_4. Analytical reagents and distilled water were used to prepare the plating solution. The nano-SiO_2, with an average particle diameter of 20 nm, was added to the electrolyte by ultrasonic vibration before electrodeposition, and the addition amount was 3g/L, mainly to refine the grains of the composite coating. $NiSO_4$ and $CoSO_4$ were the main salts of the electrolyte. $NiCl_2$ prevented the passivation of the anode. H_3BO_4 adjusted the pH of the electrolyte to 5.0. Copper was used as the cathode substrate with a size of 10 mm× 10 mm × 0.2 mm. It was polished with sandpaper and placed in dilute hydrochloric acid to remove the surface oxide layer before the experiment. The substrate was deposited in a constant current mode. The current density was calculated based on the nozzle exit size of jet electrodeposition. Table 1 shows the operating conditions of scanning jet electrodeposition.

Table 1. Operating conditions of scanning jet electrodeposition.

Operating conditions	Value
Temperature (°C)	50
Machining gap (mm)	4.0
Scanning speed (mm/s)	6.0
Electrolyte flow rate (L/h)	100
Plating time (min)	25
Current densities(A/dm^2)	70/100/130/160/190

2.3 Characterization

The surface morphology of the Co–Ni/SiO$_2$ alloy composite coating was observed by the field emission scanning electron microscope (Hitachi S-4800). The element distribution was determined by energy dispersive spectroscopy (Oxford INCA) to evaluate the element content and distribution in the alloy coating. The texture orientation of the coating was tested by the X-ray diffractometer (DMAX-2500PC), and the average grain size of the coating was estimated according to the Scherrer formula. The test conditions were 40 kV and 150 mA by Cu-Kα radiation (λ=1.5406 Å) to determine the phase composition and crystallite size. The microhardness of the coatings was measured with a Micro-hardness Tester (LEITZ Mini-Load Vickers) with the diamond tester tip and a maximum applied load of 500 g, at an applied load of 100 g for 20 s. The coating adhesion force was evaluated using the friction method with a scratch instrument (WS-2005). The load was 30 N with a rate of 30 N/min, the length of the scratches was 3 mm, the length of the dead load was 2 mm, the reciprocation frequency was 1 Hz, and the static pressure time was 30 s. Five measurements were conducted on each sample and the results were averaged to obtain the coating micro-hardness and adhesion force. The wear resistance of the composite coating was tested by the friction and wear tester (MMW-1), the load was 40N, and the wear time was 5mins. The corrosion behavior of the coatings was investigated by potentiodynamic polarization on an electrochemical workstation (CHI660C) by using a 3.5 wt% NaCl corrosive medium without agitation at room temperature. The reference electrode was a saturated calomel electrode, and the counter electrode was a platinum electrode. The samples were immersed in the corrosive medium for about 30 mins to attain the open circuit potential (Eocp). Potentiodynamic sweeping was then performed in the potential range of ±500 mV for the Eocp at a sweep rate of 1 mV/s.

3 Results and Discussion

3.1 Morphologies

Fig. 2 indicates the surface morphologies of the Co–Ni alloy composite coatings under different current densities. The surface morphologies of the coatings change significantly with the current density. When the processing current density was as low as 70 A/dm^2, the surface of the Co–Ni/SiO$_2$ alloy composite coating presented as sparse and slender structures, as shown in Fig. 2a. Fig. 2b shows that the sparse structures decreased and began to grow in a starfish crystal structure on the Co–Ni/SiO$_2$ alloy composite coating when the current density was increased to 100 A/dm^2. Fig. 2c shows that the porosity of the alloy composite coating decreased and the structure became much denser at 130 A/dm^2. However, as the current density exceeds 130 A/dm^2, in Fig. 2d (160 A/dm^2) and Fig. 2e (190 A/dm^2), some microcracks occurred at the grain boundaries of the Co–Ni/SiO$_2$ alloy composite coatings.
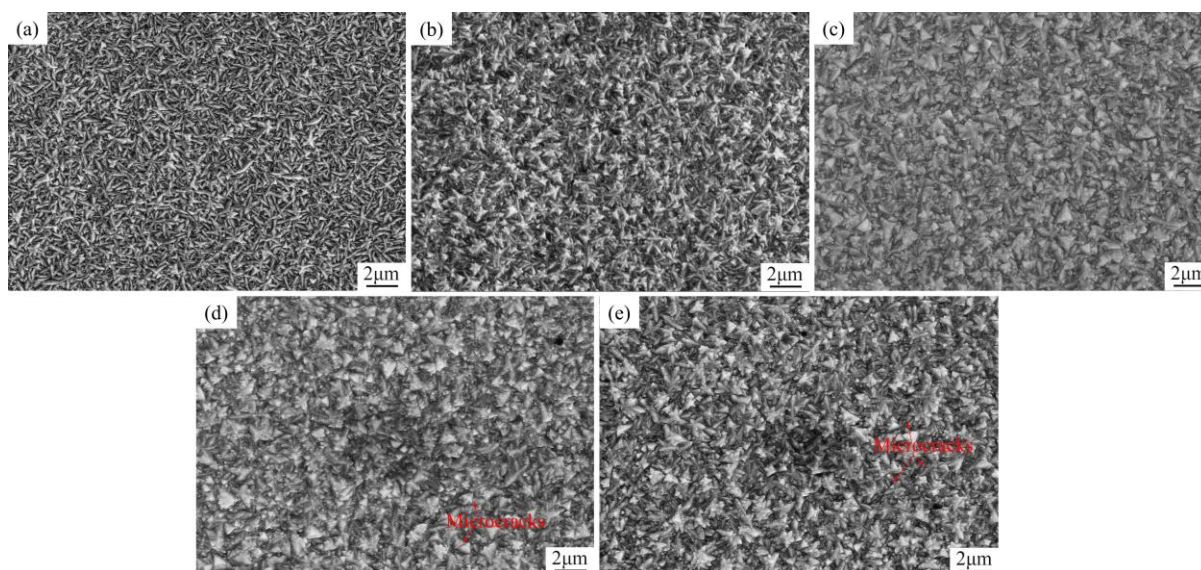
Fig. 2. Surface morphologies of Co–Ni/SiO$_2$ alloy composite coatings under different current densities.
(a) 70 A/dm^2, (b) 100 A/dm^2, (c) 130 A/dm^2, (d) 160 A/dm^2, (e) 190 A/dm^2

Fig. 3 shows the composition of the Co–Ni/SiO$_2$ alloy composite coating deposited by scanning jet electrodeposition at 130 A/dm^2. Ni and Co elements were uniformly distributed in the composite coating, while O and Si elements were relatively sparse, which was related to the concentration of nano-SiO$_2$ in the electrolyte in scanning jet electrodeposition.
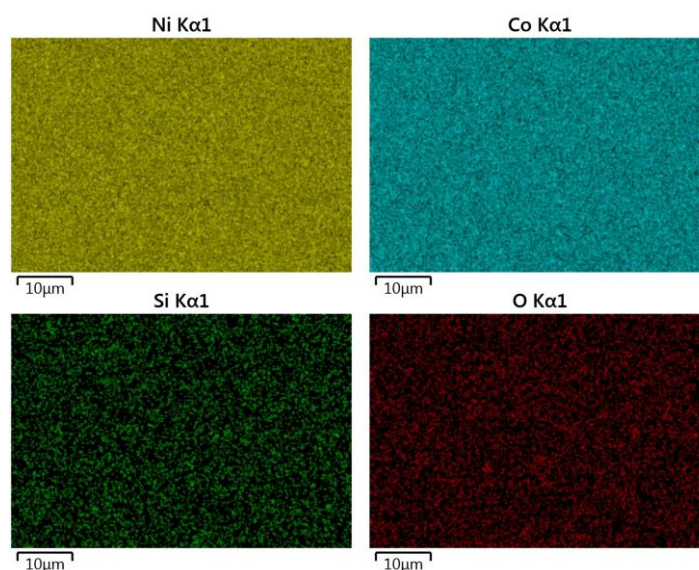

Fig. 3. Element distribution on the surface of the Co–Ni/SiO$_2$ alloy composite coating deposited by scanning jet electrodeposition at 130A/dm^2.

In the scanning jet electrodeposition, there was an abnormal co-deposition of Ni^{2+} and Co^{2+} in the electrolyte [7, 20]. Co^{2+} was deposited more easily than Ni^{2+}, and the amount of Co precipitation increased with the current density, the sparse and slender structures transformed to dense starfish structures exceeds 70A/dm^2, improving the density of the alloy composite coating. The high-speed flowing electrolyte reduced the thickness of the diffusion layer in the scanning jet electrodeposition, and the scanning movement had a refreshing effect on the discharge points on the electrode surface [15], so that the fast-growing crystal grain tips on the cathode surface were broken and their continuous growth was inhibited. Some broken grains

filled the sparse gaps on the cathode surface and provided more discharge points on the electrode surface and continued to grow, thereby improving the density of the coating. However, The electrode surface reaction rate was too fast, when the current density exceeded the optimum current density (130A/dm^2). The internal stress of the coating growth was too large, causing some microcracks to appear in the coating surface, reducing the surface quality.

3.2 Texture orientation

Fig. 4 shows the XRD patterns of the Co–Ni/SiO$_2$ alloy composite coatings under different current densities. The Co–Ni alloy composition of the Co–Ni/SiO$_2$ alloy composite coating was in the form of a solid solution and composed of a face-centered cubic (FCC) structure and a hexagonal close-packed (HCP) structure. The alloy composite coatings underwent a significant phase change in co-deposition as the current density increased [19]. The (220) diffraction peak in the Co–Ni/SiO$_2$ composite coating became narrower and sharper, which showed that the Co–Ni/SiO$_2$ composite coating had a high degree of crystallinity.
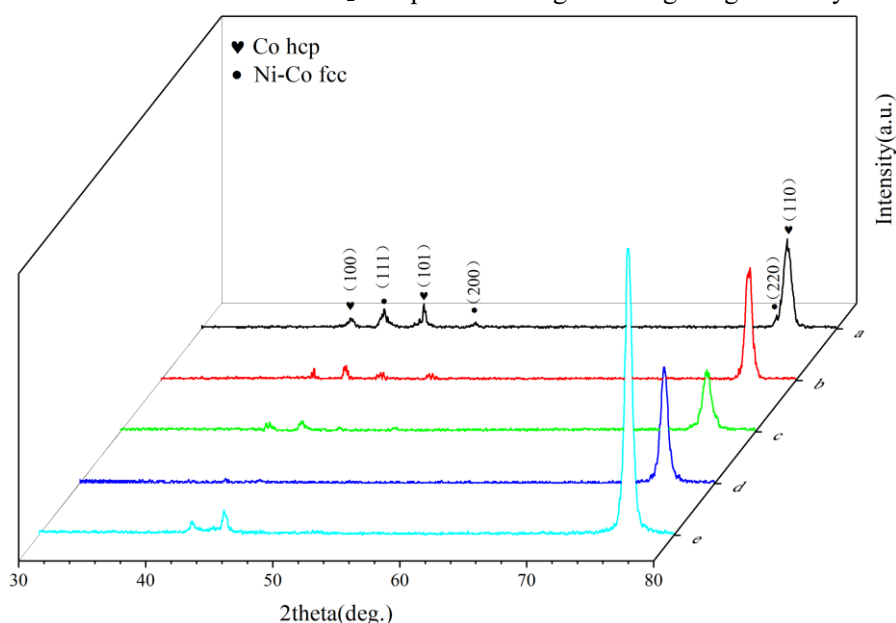

Fig. 4. XRD patterns of the different Co–Ni/SiO$_2$ alloy composite coatings.
(a) 70 A/dm^2, (b) 100 A/dm^2, (c) 130 A/dm^2, (d) 160 A/dm^2, (e)190 A/dm^2
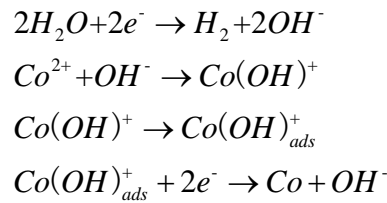
Table 2 shows the average grain size and the Co content in different Co–Ni/SiO$_2$ alloy composite coatings. The average grain size of the composite coating decreased initially before increased with the current density. The nucleation probability of the electrode surface increased with the current density, leading to a refining of the crystal grains. It was also easy to induce continuous strengthening growth when the current density was too large, as a result of which the grains of the composite coating coarsened [21].

Table 2. The average grain size of the different Co–Ni/SiO$_2$ alloy composite coatings.
(a) 70 A/dm^2, (b) 100 A/dm^2, (c) 130 A/dm^2, (d) 160 A/dm^2, (e)190 A/dm^2

Samples	Average grain size (nm)	Co (wt%)	SiO$_2$ (wt%)
a	34.8	56.3	1.20
b	19.7	58.1	2.63
c	17.8	59.8	3.27
d	18.7	61.4	2.89
e	21.8	62.7	2.54

It can be seen from the Co content in wt% in the composite coating in Table 2 that the content ratio of Co to Ni in the composite coating is much greater than the concentration ratio of Co^{2+} to Ni^{2+} in the electrolyte because abnormal co-deposition occurred during scanning jet electrodeposition. This was similar to related electrodeposition research [22, 23]. Besides, The content of nanoparticles in the composite coating also changes to a certain extent under different current densities, and the amount of embedded nanoparticles increases as the content of Co increases. In the Co-Ni alloy co-deposition, the pH value near the cathode increased due to the precipitation of hydrogen. In the process of electrodeposition, hydrogen was released by electrolysis of water, which also increased the pH near the cathode. When the pH was high enough near the cathode, metal hydroxide would be produced to hinder the electrodeposition. The abnormal co-deposition could be considered as the hydroxide colloid produced in the electrodeposition process hindering the normal deposition process. According to the theory of abnormal co-deposition, due to the increase of pH on the cathode surface in the electrodeposition, the active metal Co^{2+} ion was easy to form $Co(OH)_2$ colloid under alkaline conditions, which adsorbed on the cathode surface and hinders the passage of nickel ion, but Co^{2+} ion could discharge through $Co(OH)_2$, resulting in the increase of cobalt content in the coating. With the increase of pH, the dispersion of Nano-SiO_2 is enhanced, and more nano-SiO_2 was embedded in the alloy coating with Co^{2+} ion deposition. However, the number of embedded nanoparticles decreased when the current density was too large, which might be due to the faster precipitation of the Co element. The nanoparticles could not be completely converted from weak adsorption to strong adsorption, and they were washed away by the high-speed electrolyte flow.

The metal ions arriving on the surface of the cathode electrode were quickly deposited when the current density on the electrode surface increased. Since jet electrodeposition provided a higher current density and accelerated the electrode surface reaction rate, Co^{2+} was much easier to precipitate, and in particular, the Co content in the composite coating further increased with current density. The reaction equation of Co–Ni alloy co-deposition was as follows [24]:

$$2H_2O+2e^- \rightarrow H_2+2OH^-$$
$$Co^{2+}+OH^- \rightarrow Co(OH)^+$$
$$Co(OH)^+ \rightarrow Co(OH)^+_{ads}$$
$$Co(OH)^+_{ads} + 2e^- \rightarrow Co+OH^-$$

3.3 Microhardness and adhesion force

Fig. 5 shows the microhardness and adhesion force of the different Co–Ni/SiO_2 alloy composite coatings. The microhardness and adhesion force of the Co–Ni/SiO_2 alloy composite coating increased with increasing current density to reach a peak at the optimum current density (130 A/dm^2). Afterward they decreased again. The composite coating exhibited the best microhardness of 5.43 GPa, and the adhesion force with the substrate was as high as 27.48 N when the current density was 130 A/dm^2.
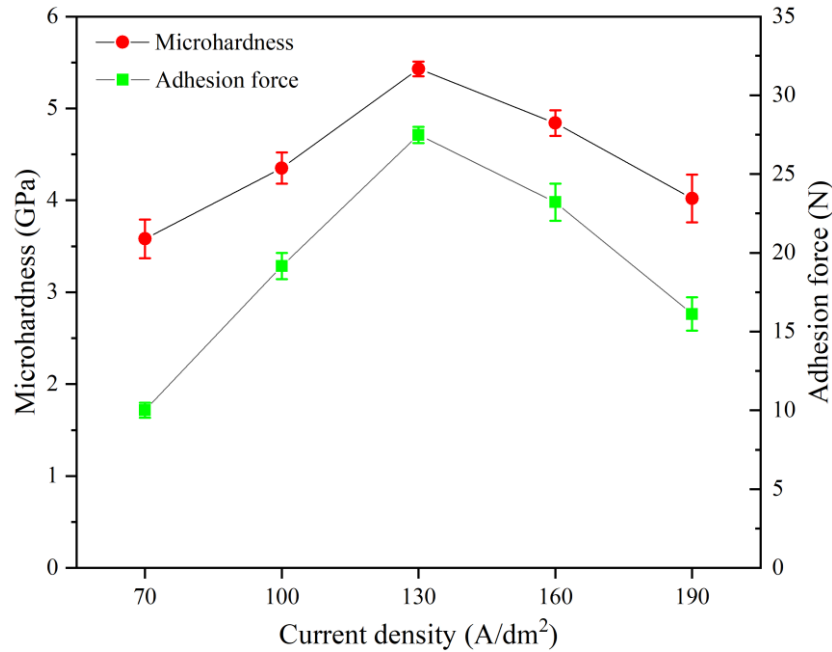
Fig. 5. Microhardness and adhesion force of the different Co–Ni/SiO₂ alloy composite coatings.
(a) 70 A/dm², (b) 100 A/dm², (c) 130 A/dm², (d) 160 A/dm², (e)190 A/dm²

The microhardness of the Co–Ni alloy composite coating gradually increased with the current density, because the grains of the Co–Ni alloy were further refined with an increase in current density. The mechanical properties of the alloy are largely related to the grain size [25, 26]. According to the Hall–Petch formula [27], the decrease in grain size increased the microhardness of the material. When the current density exceeds the optimum current density, the microhardness of the coating decreased. A further increase in current density produces a high-stress coating, which causes crystal deformation and microcracks. In addition, when the optimum current density was exceeded, the hydrogen evolution near the electrode surface was aggravated. If the hydrogen could not be released in time, it was enclosed in the coating to form pore defects [28], thereby reducing the microhardness and adhesion force.

3.4 Wear resistance

Fig. 6 illustrates the surface morphologies of the coating under different current densities after wear. Fig. 6a shows that the Co–Ni/SiO₂ alloy composite coating has an obvious furrow when the current density was 70 A/dm², the coating was torn off and accompanied by a large amount of wear debris, which had a very poor wear resistance [29]. Fig. 6b shows that the Co–Ni/SiO₂ alloy composite coating has many wear debris, delamination, and grooves parallel to the direction of frictional movement. The wear mechanism was mainly abrasive wear with the current density added to 100 A/dm². Fig. 6c shows the surface morphology of the alloy coating after wear is relatively complete, with few pits, when the current density increased to 130 A/dm², it showed the best wear resistance in the wear test. However, in Fig. 6d, the wear resistance of the Co–Ni/SiO₂ alloy composite coating was reduced with micro-cracks, and the grooves were visible with the current density of 160 A/dm². Especially in Fig. 6e, the Co–Ni/SiO₂ alloy composite coating has large cracks and a small amount of delamination at 190 A/dm².

Therefore, it can be explained that the friction and wear characteristics of the alloy composite coating were closely related to the optimum current density. The decrease of the coating density and the change of the microstructure are the important reasons for the poor wear resistance of the alloy composite coating, which was easily damaged during the friction process. However, the alloy composite coating deposited too

fast at a much higher current density, then the internal stress was too large, and cracks were prone to occur during the wear process, which led to reduce wear resistance of Co–Ni/SiO$_2$ alloy composite coating.
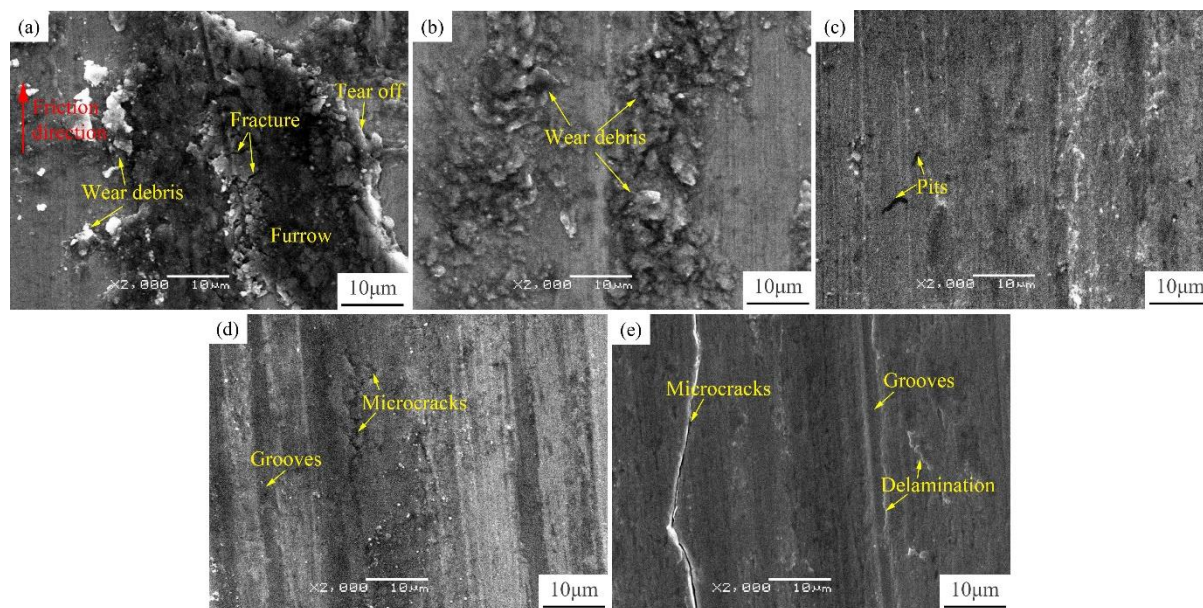

Fig. 6. Surface morphologies of the coating under different current densities after wear.
(a) 70 A/dm^2, (b) 100 A/dm^2, (c) 130 A/dm^2, (d) 160 A/dm^2, (e)190 A/dm^2

3.5 Corrosion resistance

Fig. 7 is the polarization curve of the Co–Ni/SiO$_2$ alloy composite coating tested in a 3.5% NaCl solution. The corrosion data obtained from the polarization curve is shown in Table 3. The corrosion resistance of the Co–Ni/SiO$_2$ composite coating showed significant improvement with a current density below the optimum current density. From Table 3, the Co–Ni/SiO$_2$ alloy composite coating exhibited excellent corrosion resistance, with a corrosion current density as low as 0.506 µA·cm^{-2}. When the current density reached 190 A/dm^2, i.e. considerably exceeding the current density (130 A/dm^2), the corrosion current density of the composite coating increased to 2.965 µA·cm^{-2}. Thus, the corrosion resistance of the composite coating decreased after exceeding the optimum current density.
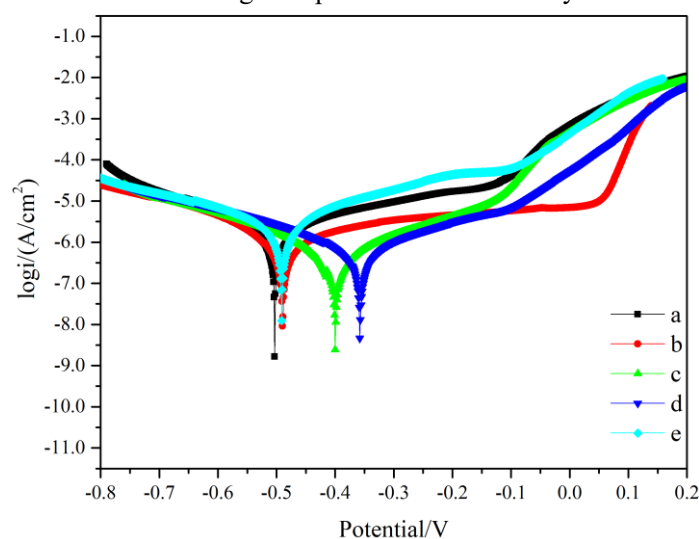

Fig. 7. Polarization curves of the different Co–Ni/SiO$_2$ alloy composite coatings.
(a) 70 A/dm^2, (b) 100 A/dm^2, (c) 130 A/dm^2, (d) 160 A/dm^2, (e)190 A/dm^2

Table 3. Electrochemical data extracted from the polarization curves.
(a) 70 A/dm^2, (b) 100 A/dm^2, (c) 130 A/dm^2, (d) 160 A/dm^2, (e)190 A/dm^2

Samples	E_{corr}/V	i_{corr}/$\mu A \cdot cm^{-2}$
a	-0.503	2.184
b	-0.490	1.133
c	-0.400	0.506
d	-0.358	0.762
e	-0.491	2.965

Fig. 8 shows the surface morphologies of the Co–Ni/SiO$_2$ alloy composite coating placed in the NaCl solution for further immersion for 144 h after the electrochemical test. Fig. 8a shows several large corrosion pits and holes on the surface of the composite coating with a lower current density (70 A/dm^2) in scanning jet electrodeposition. In Fig. 8b (130 A/dm^2), the Co–Ni/SiO$_2$ composite coating was preserved relatively well, and there were no corrosion pits and holes, indicating better corrosion resistance.
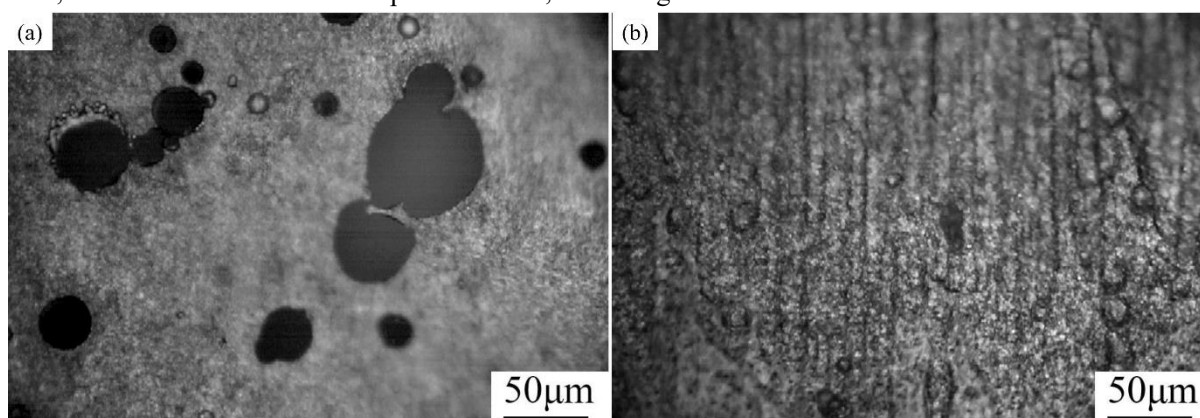

Fig. 8. Morphologies of Co–Ni/SiO$_2$ alloy composite coating after immersion for 144h.
(a) 70 A/dm^2, (b) 130 A/dm^2.

The corrosion of materials is usually because the corrosive medium penetrates the interior through the holes and microcracks on the surface of the composite coating [18, 30]. Therefore, the density of the composite coating has an important influence on the corrosion protection of the composite coating. Combined with the surface morphologies of the alloy composite coatings in Fig. 2, the denser composite coating has better corrosion resistance. When the current density was as low as 70 A/dm^2, the surface micromorphology of the Co–Ni/SiO$_2$ composite coating was looser and the compactness was poor. For current densities below the optimum current density, the surface morphologies of the composite coatings became denser with increasing current density. Denser coatings prevent the penetration of corrosive liquids, thereby enhancing the corrosion resistance of the composite coating. Once the current density exceeded the optimum current density (Table. 3d and e), the deposition rate of Co^{2+} and Ni^{2+} near the electrode surface on the substrate occurred so fast that microcracks occurred on the composite coating. These microcracks decrease the compactness due to excessive internal stress, which provided corrosion channels for the penetration of the electrolyte. Some pores were formed in the coating due to the hydrogen evolution at a higher current density. The trapping of the hydrogen bubbles reduced the compactness of the coating. Once the corrosive solution penetrated the coating, it further accelerated the corrosion, and the corrosion resistance worsened [31].

4 Conclusion

This paper studied the impact of the current density onto the Co–Ni/SiO$_2$ alloy composite coating in scanning jet electrodeposition. It was found that the surface morphologies of the alloy composite coatings changed from sparse and slender structures toward dense starfish structures upon increasing the current density. Furthermore, the best values of microhardness (5.43 GPa) and adhesion force (27.48 N), as well as a low corrosion current density (0.506 $\mu A \cdot cm^{-2}$), can be achieved under the current density of 130 A/dm^2. Once the current density was exceeded, the microhardness, adhesion force, and corrosion resistance of the alloy composite coating decreased again due to excessive internal stress.

Reference

[1] S.I. Ghazanlou, A.H.S. Farhood, S. Hosouli, S. Ahmadiyeh, A. Rasooli, Pulse and direct electrodeposition of Ni–Co/micro and nanosized SiO$_2$ particles, Mater. Manuf. Process. 33 (2017) 1067-1079.

[2] F. Cai, X. Cai, S. Zhang, C. Jiang, Microstructure evolution and improved corrosion resistance of electrodeposited NiCo–Al composite coatings with different Al contents, J. Alloy. Compd. 738 (2018) 72-78.

[3] S.I. Ghazanlou, S. Ahmadiyeh, R. Yavari, Investigation of pulse electrodeposited Ni–Co/SiO$_2$ nanocomposite coating, Surf. Eng. 33 (2017) 337-347.

[4] M.S. Safavi, M. Tanhaei, M.F. Ahmadipour, R.G. Adli, S. Mahdavi, F.C. Walsh, Electrodeposited Ni–Co alloy-particle composite coatings: A comprehensive review, Surf. Coat. Technol. 382 (2020) 125153.

[5] B. Li, W. Zhang, Electrochemical Deposition of Ni–Co/SiC Nanocomposite Coatings for Marine Environment, Int. J. Electrochem. Sci. 2017, 12(8) 7017-7030.

[6] S. Singh, S. Samanta, A.K. Das, R.R. Sahoo, Tribological investigation of Ni-graphene oxide composite coating produced by pulsed electrodeposition, Surf. Interfaces, 12 (2018) 61-70.

[7] M.A.M. Ibrahim, R.S. Bakdash, Copper-rich Cu–Zn alloy coatings prepared by electrodeposition from glutamate complex electrolyte: Morphology, structure, microhardness and electrochemical studies, Surf. Interfaces, 18 (2020) 100404.

[8] V.R.C. Thanu, C. Andrew, M. Jayakumar, Electrodeposition Of Nickel Super Alloy From Deep Eutectic Solvent, Surf. Interfaces, 19 (2020) 100539.

[9] Y. Wu, Z. Zhang, K. Xu, J. Lu, X. Dai, H. Zhu, S. Yang, Effect of Laser Single Pulse Energy on Micro-structural, Mechanical and Corrosion Properties of Amorphous Ni-Fe-P Alloy Prepared by Laser-Assisted Electrodeposition, Surf. Interfaces, 22 (2021) 100811.

[10] P. Shahmohammadi, B. A. Khazaei, Characterization of Zn/Mg-enriched calcium phosphate coating

produced by the two-step pulsed electrodeposition method on titanium substrate, Surf. Interfaces, 22 (2021) 100819.

[11] S. Das, S. Banthia, A. Patra, S. Sengupta, S.B. Singh, Novel bilayer Zn–Ni/Ni–Co–SiC nanocomposite coating with exceptional corrosion and wear properties by pulse electrodeposition, J. Alloy. Compd. 738 (2018) 394-404.

[12] B. Bahadormanesh, A. Dolati, M.R. Ahmadi, Electrodeposition and characterization of Ni–Co/SiC nanocomposite coatings, J. Alloy. Compd. 509 (2011) 9406-9412.

[13] N. Fenineche, A.M. Chaze, C. Coddet, Effect of pH and current density on the magnetic properties of electrodeposited Co–Ni–P alloys, Surf. Coat. Technol. 88 (1997) 264-268.

[14] A.R. Shetty, A.C. Hegde, Ultrasound induced multilayer Ni–Co alloy coatings for better corrosion protection, Surf. Coat. Technol. 322 (2017) 99-107.

[15] C. Wang, L. Shen, M. Qiu, Z. Tian, W. Jiang, Characterizations of Ni–CeO$_2$ nanocomposite coating by interlaced jet electrodeposition. J. Alloy. Compd. 727 (2017) 269-277.

[16] Y. Wang, L. Shen, M. Qiu, Z. Tian, X. Liu, W. Zhuo, Jet Electrodeposition of Ni–SiO$_2$ Nanocomposite Coatings with Online Friction and Its Performance, J. Electrochem. Soc. 163 (2016) 579-584.

[17] W. Jiang, L. Shen, M. Qiu, X. Wang, M. Fan, Z. Tian, Preparation of Ni–SiC composite coatings by magnetic field-enhanced jet electrodeposition, J. Alloy. Compd. 762 (2018) 115-124.

[18] K. Zhao, L. Shen, M. Qiu, Z. Tian, W. Jiang, Preparation and Properties of Nanocomposite Coatings by Pulsed Current-Jet Electrodeposition. Int. J. Electrochem. Sci. 12 (2017) 8578-8590.

[19] Q. Zhang, J. Tan, L. Meng, F. Xie, H. Zhao, Z. Yan, Preparation of Co–Ni Alloy Coating with Stable Composition by Jet-Electrodeposition. Appl. Sci. 9 (2019) 5545.

[20] J. Matulis, R. Sližys, On some characteristics of cathodic processes in nickel electrodeposition, Electrochim. Acta 9 (1964) 1177-1188.

[21] B. Li, D. Li, W. Chen, Y. Liu, J. Zhang, Y. Wei, W. Zhang, W. Jia, Effect of current density and deposition time on microstructure and corrosion resistance of Ni–W/TiN nanocomposite coating, Ceram. Int. 45 (2019) 4870-4879.

[22] S. Hessami, C.W. Tobias, A Mathematical Model for Anomalous Codeposition of Nickel-Iron on a Rotating Disk Electrode, J. Electrochem. Soc. 136 (1989) 3611-3616.

[23] H. Dahms, I. Croll, The Anomalous Codeposition of Iron–Nickel Alloys, J. Electrochem. Soc. 112 (1965) 771-775.

[24] D. Grimmett, M. Schwartz, K. Nobe, Pulsed Electrodeposition of Iron–Nickel Alloys, J. Electrochem. Soc. 137 (1990) 3414-3418.

[25] B. Li, W. Zhang, Y. Huan, J. Dong, Synthesis and characterization of Ni–B/Al$_2$O$_3$ nanocomposite coating by electrodeposition using trimethylamine borane as boron precursor, Surf. Coat. Technol. 337 (2018) 186-197.

[26] A. Akbari, R. Mohammadzadeh, Effect of Grain Refinement on the Mechanical Properties of a Nickel- and Manganese-Free High Nitrogen Austenitic Stainless Steel, Metall. Mater. Trans. A 46 (2015) 1570-1579.

[27] R. Mahmudi, Grain boundary strengthening in a fine grained aluminium alloy, Scripta Meta. 32 (1995) 781-786.

[28] L. Ren, Y. Cheng, Z. Han, X. Meng, J. Yang, Investigation on the mechanical performance of the electroless Ni-W-P coating based on fractal theory, Surf. Topogr.: Metrol. Prop. 7 (2019) 025017.

[29] S. Kheirkhah, M. Imani, R. Aliramezani, M.H. Zamani, A. Kheilnejad, Microstructure, mechanical properties and corrosion resistance of Al6061/BN surface composite prepared by friction stir processing, Surf. Topogr.: Metrol. Prop. 7 (2019) 035002.

[30] S Dehgahi, R Amini, M. Alizadeh, Microstructure and corrosion resistance of Ni–Al$_2$O$_3$–SiC nanocomposite coatings produced by electrodeposition technique, J. Alloys Compd. 692 (2017) 622-

628.

[31] Y. Yang, Y.F. Cheng, Mechanistic aspects of electrodeposition of Ni–Co–SiC composite nano-coating on carbon steel, Electrochim. Acta 109 (2013) 638-644.